

## Atomic Layer Deposition

International Edition: DOI: 10.1002/anie.201700449  
German Edition: DOI: 10.1002/ange.201700449

## Atomic Layer Deposition of Iron Sulfide and Its Application as a Catalyst in the Hydrogenation of Azobenzenes

Youdong Shao<sup>+</sup>, Zheng Guo<sup>+</sup>, Hao Li, Yantao Su, and Xinwei Wang\*

**Abstract:** The atomic layer deposition (ALD) of iron sulfide (FeS<sub>x</sub>) is reported for the first time. The deposition process employs bis(*N,N'*-di-*tert*-butylacetamidinato)iron(II) and H<sub>2</sub>S as the reactants and produces fairly pure, smooth, and well-crystallized FeS<sub>x</sub> thin films following an ideal self-limiting ALD growth behavior. The FeS<sub>x</sub> films can be uniformly and conformally deposited into deep narrow trenches with aspect ratios as high as 10:1, which highlights the broad applicability of this ALD process for engineering the surface of complex 3D nanostructures in general. Highly uniform nanoscale FeS<sub>x</sub> coatings on porous  $\gamma$ -Al<sub>2</sub>O<sub>3</sub> powder were also prepared. This compound shows excellent catalytic activity and selectivity in the hydrogenation of azo compounds under mild reaction conditions, demonstrating the promise of ALD FeS<sub>x</sub> as a catalyst for organic reactions.

Iron sulfide (FeS<sub>x</sub>) is an important earth-abundant material that has recently received great attention for a variety of applications, such as solar cells,<sup>[1]</sup> lithium-ion batteries,<sup>[2]</sup> and as a catalyst for hydrogen evolution,<sup>[3]</sup> oxygen reduction,<sup>[4]</sup> CO<sub>2</sub> reduction,<sup>[5]</sup> and organic synthesis.<sup>[6]</sup> Many of these applications are based on the use of nanostructured FeS<sub>x</sub> as the active material<sup>[7]</sup> as nanostructured materials usually have a fairly large surface area and thus expose a large number of active sites, which can considerably boost the performance of active materials. To fabricate nanostructured FeS<sub>x</sub>, many synthetic methods, including solution-based methods,<sup>[2a,c,3c,d,4]</sup> mechanical ball milling,<sup>[2b]</sup> gas-phase sulfidation,<sup>[8]</sup> and chemical vapor deposition,<sup>[1c,9]</sup> have been adopted in the past. On the other hand, atomic layer deposition (ALD) has recently gained significant attention as a highly useful deposition technique for fabricating nanostructured materials.<sup>[10]</sup> ALD employs saturated, self-limiting surface-chemistry reactions and allows the designed materials to grow in a layer-by-layer fashion<sup>[11]</sup> so that, in theory, any complex 3D structure can be conformally and uniformly coated by ALD with excellent reproducibility and atom-precise control over the film composition and thickness. These unique features of ALD have recently enabled a variety of studies<sup>[12]</sup> on the fabrication and engineering of nanomaterials, especially for the nanoscale engineering of the surface of complex 3D scaffold

electrodes, which have shown great promise for energy conversion and storage applications.<sup>[12]</sup> Meanwhile, ALD has also been regarded as an exceptionally powerful tool for catalyst design.<sup>[13]</sup> Taking advantage of the atomic precision of this method, ALD has been used to create catalyst materials with well-controlled, homogeneous distributions in terms of their sizes, compositions, and active sites, which can not only improve the activity, selectivity, and stability of the catalysts, but also significantly facilitate the elucidation of the reaction mechanisms and catalyst structure–property relationships.<sup>[13]</sup> Moreover, a variety of new catalyst structures for high-performance multifunctional catalysis have recently been enabled by ALD.<sup>[14]</sup> Over the past decades, the ALD technique itself has been developing very rapidly with hundreds of different materials having been synthesized by ALD.<sup>[15]</sup> However, as reviewed recently,<sup>[16]</sup> there is still no ALD process for the synthesis of FeS<sub>x</sub> materials. Considering the important and broad applications of FeS<sub>x</sub>, the absence of an ALD process for its synthesis can seriously limit the advancement of FeS<sub>x</sub>-based nanoscale engineering for electro- and chemical catalysis. Therefore, the development of a new ALD process for FeS<sub>x</sub> is urgently required.

Herein, we report the first ALD process for FeS<sub>x</sub>. The process employed bis(*N,N'*-di-*tert*-butylacetamidinato)iron(II) (Fe(amd)<sub>2</sub>, Figure 1) and H<sub>2</sub>S as the reactants, and

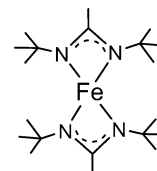


Figure 1. Structure of bis(*N,N'*-di-*tert*-butylacetamidinato)iron(II).

followed ideal self-limiting ALD growth behavior over a wide temperature range to produce fairly pure, smooth, and well-crystallized FeS<sub>x</sub> films. The ALD FeS<sub>x</sub> films were conformally deposited into deep narrow trenches with aspect ratios as high as 10:1, which indicated that this ALD process is highly suitable for preparing conformal and uniform FeS<sub>x</sub> coatings on general 3D complex or porous nanostructures. We also fabricated nanoscale FeS<sub>x</sub> coatings on porous  $\gamma$ -Al<sub>2</sub>O<sub>3</sub> powder by ALD, and used the prepared FeS<sub>x</sub> catalyst for the selective reduction (hydrogenation) of azobenzenes to hydrazobenzenes. As hydrazobenzenes generally suffer from facile reductive cleavage of the NH–NH bond to form amines, the selective reduction of azo to hydrazo compounds is important and needs special care.<sup>[17]</sup> With our FeS<sub>x</sub> catalyst prepared by ALD, we achieved the selective reduction (hydrogenation) of

[\*] Dr. Y. Shao,<sup>[†]</sup> Z. Guo,<sup>[†]</sup> H. Li, Dr. Y. Su, Prof. Dr. X. Wang  
School of Advanced Materials  
Shenzhen Graduate School, Peking University  
Shenzhen 518055 (China)  
E-mail: wangxw@pkusz.edu.cn

[†] These authors contributed equally to this work.

Supporting information for this article can be found under:  
<http://dx.doi.org/10.1002/anie.201700449>.

azobenzenes with electron-withdrawing or -donating groups with high activity and selectivity under mild reaction conditions.

The ALD of  $\text{FeS}_x$  was carefully investigated at deposition temperatures ranging from 80 to 300 °C. Unless otherwise specified, UV/ozone-treated planar Si wafer substrates (with a ca. 1 nm thick  $\text{SiO}_2$  surface layer) were used to study the deposition behavior. Typical self-limiting ALD growth behavior was observed for deposition temperatures of up to 200 °C. Representative thickness saturation curves for films deposited at 120 °C by 400 ALD cycles at various precursor dosages are shown in Figure 2a,b. As shown in Figure 2a, the film thickness first increased with the  $\text{Fe}(\text{amd})_2$  exposure, and then reached saturation as the  $\text{Fe}(\text{amd})_2$  exposure exceeded about 0.025 Torr s while the amount of  $\text{H}_2\text{S}$  was kept fixed at approximately 0.062 Torr s. Similarly, as shown in Figure 2b, when the amount of  $\text{Fe}(\text{amd})_2$  was kept fixed at about 0.025 Torr s, the film thickness also increased initially and then reached saturation as the  $\text{H}_2\text{S}$  exposure exceeded approximately 0.062 Torr s. These results clearly indicate that saturated, self-limiting film growth could be achieved with minimum exposures of about 0.025 and 0.062 Torr s for  $\text{Fe}(\text{amd})_2$  and  $\text{H}_2\text{S}$ , respectively. Under saturation conditions, the thickness of the deposited film follows an ideal linear relation with the total number of ALD cycles, suggesting good linear growth behavior for this ALD process (Figure 2c). Good growth linearity is of particular importance for ALD as it could enable one to precisely control the thickness of deposited films by simply varying the total number of ALD cycles. In addition, the linear fit shown in Figure 2c also revealed a negligible intercept, which suggests negligible nucleation delay in this ALD process.

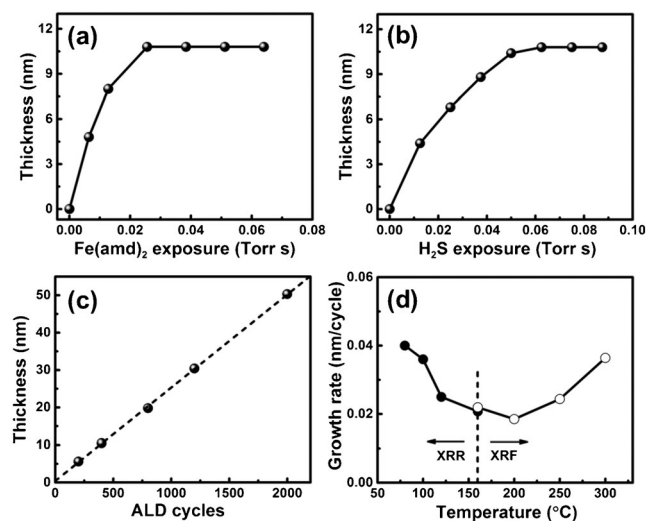


**Figure 2.** a) Film thickness with respect to  $\text{Fe}(\text{amd})_2$  exposure at a fixed  $\text{H}_2\text{S}$  exposure of about 0.062 Torr s. b) Film thickness with respect to  $\text{H}_2\text{S}$  exposure at a fixed  $\text{Fe}(\text{amd})_2$  exposure of about 0.025 Torr s. Total number of ALD cycles in (a) and (b): 400 cycles. c) Film thickness as a function of the number of ALD cycles. A deposition temperature of 120 °C was used in (a)–(c). d) Growth rate as a function of the deposition temperature. The corresponding film thickness was measured by XRR (●) and/or XRF (○).

The temperature dependence of the growth rate is plotted in Figure 2d. The film thickness, which was used to calculate the growth rate, was directly measured by X-ray reflectometry (XRR) for films deposited at  $\leq 160$  °C, but for higher deposition temperatures ( $\geq 160$  °C), the deposited films were too rough (see below) to be analyzed by XRR; therefore, X-ray fluorescence (XRF) was used instead to estimate the thickness. XRF measures the areal density of each element in the film, which can be used to calculate the areal mass of the deposited film. Assuming a film density of  $4.83 \text{ g cm}^{-3}$  (the bulk density of stoichiometric  $\text{FeS}$ , PDF No. 37-0477), the film thickness could therefore be calculated. The correctness of this bulk density assumption was confirmed for the films deposited at 160 °C as the values of the growth rates obtained by XRR and XRF agreed well with each other (Figure 2d). The growth rate was found to decrease from 0.40 to 0.19 Å per cycle as the temperature was increased from 80 to 200 °C, and then started to increase above 250 °C, which implies that the precursors undergo partial decomposition at high temperatures.

The film microstructures and crystallinity were examined by transmission electron microscopy (TEM). As shown in Figure 3a–d, the ALD  $\text{FeS}_x$  films were well-crystalline for all deposition temperatures from 80 to 250 °C. However, the crystallinity depended on the deposition temperature as the electron diffraction patterns for low-temperature ( $\leq 120$  °C) and high-temperature ( $\geq 160$  °C) ALD films were pronouncedly different (Figure 3e). After careful comparison with reference compounds (see the Supporting Information, Figure S1), the low- and high-temperature ALD  $\text{FeS}_x$  films were determined to correspond to mackinawite (tetragonal) and pyrrhotite (hexagonal or monoclinic) phases, respectively. The temperature dependence of the phase formation implies that under our ALD conditions, the pyrrhotite was thermodynamically more stable than the mackinawite. In fact, the phase transition of  $\text{FeS}_x$  from mackinawite to pyrrhotite is often observed in geochemistry,<sup>[18]</sup> where mackinawite is the

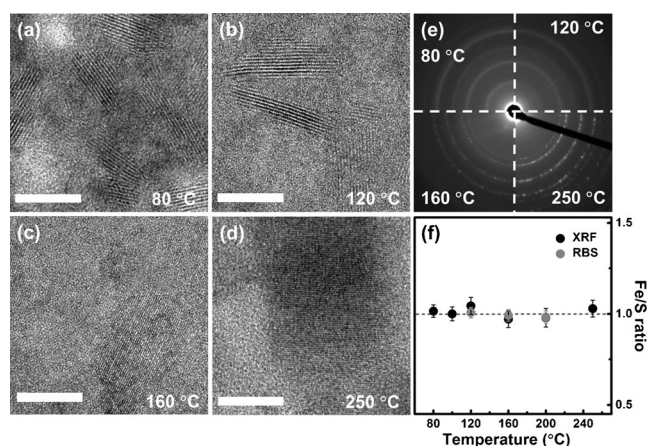


**Figure 3.** TEM images of approximately 20 nm thick  $\text{FeS}_x$  films deposited at a) 80, b) 120, c) 160, and d) 250 °C. Scale bars: 10 nm. e) The associated electron diffraction patterns. The ALD  $\text{FeS}_x$  films were all deposited on UV/ozone-treated  $\text{SiN}_x$  grids for TEM. f) Fe/S atomic ratio as a function of the deposition temperature.

iron sulfide formed first in most ambient environments, and then converts into more stable iron sulfide phases such as pyrrhotite.<sup>[19]</sup> The similar phase behavior under the ALD vacuum conditions and in aqueous geochemistry is remarkable. In addition, as ALD processes are known for their high reproducibility, this well-behaved temperature dependence of the phase of the crystalline film should enable controlling the highly reproducible formation of uniform phases by simply adjusting the deposition temperature.

The Fe/S atomic ratios in the ALD films were determined by both XRF and Rutherford backscattering spectroscopy (RBS). As shown in Figure 3 f, the Fe/S ratio was fairly close to 1.0 for all deposition temperatures. A stoichiometry of 1:1 had indeed been expected as both Fe and S are divalent in their respective precursors. However, considering the accuracy of the measurements (ca. 5%), we cannot completely exclude the possibility that the actual atomic ratios deviate a few percent from the 1:1 stoichiometry, especially considering that both mackinawite and pyrrhotite phases can accommodate fairly large deviations from the 1:1 stoichiometry (up to ca. 10%).<sup>[18,20]</sup>

The purity of the ALD films was further analyzed by X-ray photoelectron spectroscopy (XPS). Prior to the XPS measurements, all samples were subjected to Ar<sup>+</sup> sputtering for 150 s to remove adventitious carbon and surface oxide. Representative survey and high-resolution XPS spectra for an approximately 20 nm thick FeS<sub>x</sub> film deposited at 160 °C are shown in Figure 4. The high-resolution Fe 2p spectrum shows

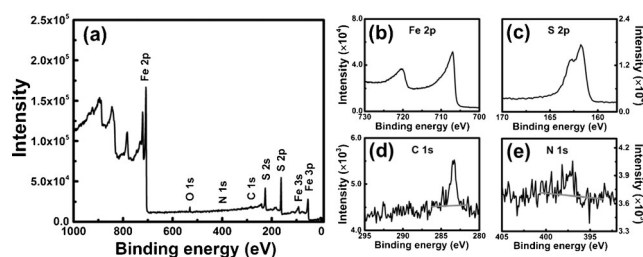


**Figure 4.** a) XPS survey spectrum for an approximately 20 nm thick FeS<sub>x</sub> film deposited at 160 °C and the associated b) Fe 2p, c) S 2p, d) C 1s, and e) N 1s high-resolution spectra.

a pair of spin-orbit-split peaks at 706.9 eV ( $2p_{3/2}$ ) and 720.3 eV ( $2p_{1/2}$ ), and the high-resolution S 2p spectrum shows a pair of spin-orbit-split peaks at 161.8 eV ( $2p_{3/2}$ ) and 162.7 eV ( $2p_{1/2}$ ), which are all consistent with the literature values for iron sulfide.<sup>[9b]</sup> Possible C and N impurities were determined to be as low as about 1.6 and 0.5 at%, respectively, which indicates that the purity of the ALD FeS<sub>x</sub> film was fairly high. Additional spectra for films deposited at different temperatures (80–250 °C) are provided in Figure S2. The impurity levels for C and N were even lower than the detection limit (ca. 0.5 at%) for higher deposition temperatures. In addition, a small oxygen peak was observed in the survey spectrum (Figure 4 a), which was due to post-oxidation of the FeS<sub>x</sub> surface upon exposure to air. An ALD Co<sub>9</sub>S<sub>8</sub> film<sup>[21]</sup> was further deposited in situ on top of the FeS<sub>x</sub> film to confirm this property (Figure S3).

The surface morphology of the FeS<sub>x</sub> films was examined by both scanning electron microscopy (SEM) and atomic force microscopy (AFM). SEM and AFM images for approximately 20 nm thick films deposited at various temperatures from 80 to 200 °C are shown in Figure 5 a–j. Granular

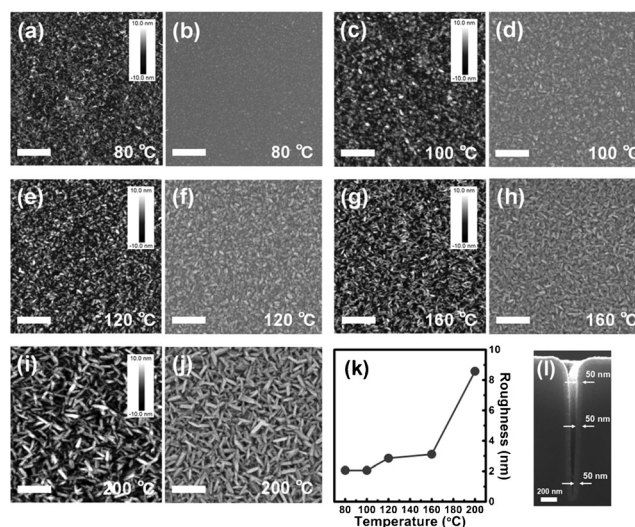


**Figure 5.** a, c, e, g, i) AFM and b, d, f, h, j) SEM images of approximately 20 nm thick FeS<sub>x</sub> films deposited at 80 °C (a, b), 100 °C (c, d), 120 °C (e, f), 160 °C (g, h), and 200 °C (i, j). Scale bars: 200 nm. k) Plot of the rms roughness as a function of the deposition temperature. l) Cross-sectional SEM image showing conformal film deposition inside a deep narrow trench with an aspect ratio as high as 10:1. The deposition was performed at 120 °C with 2000 ALD cycles.

features are clearly visible in all of these images, suggesting that the as-deposited films were all polycrystalline. The root mean square (rms) roughness was plotted in Figure 5 k as a function of the deposition temperature. FeS<sub>x</sub> films deposited below 160 °C were generally smooth as their rms roughness (2–3 nm) amounted to only about 10–15% of their film thickness (ca. 20 nm). However, when the deposition temperature exceeded 160 °C, the films started to form flake-shaped crystallites with increased surface roughness (Figure 5 i, j).

The FeS<sub>x</sub> films could also be conformally deposited into deep narrow trenches with high aspect ratios. As demonstrated by the cross-sectional SEM image in Figure 5 l, for a 1.85 μm deep trench with a high aspect ratio of 10:1, the deposited FeS<sub>x</sub> film was able to conformally cover the entire trench with uniform thickness throughout the trench. This high conformality is an important feature of a good ALD process in which the surface chemistry reactions are indeed self-limiting, and it also indicates that this ALD process can be employed to uniformly coat FeS<sub>x</sub> films onto highly porous structures or complex 3D structures with high aspect ratios.

Thus far, we have shown that with our ALD process, we can produce pure, smooth FeS<sub>x</sub> thin films with excellent conformality and precise thickness control. We were then interested in using this approach to uniformly coat γ-Al<sub>2</sub>O<sub>3</sub> powder with a FeS<sub>x</sub> thin layer for applications in organic synthesis. FeS<sub>x</sub> is assumed to be a good catalyst as many

enzymes contain active Fe–S clusters for catalyzing biological organic transformations.<sup>[6a]</sup>

To this end, a thin layer of FeS<sub>x</sub> (ca. 30 nm) was deposited on activated porous  $\gamma$ -Al<sub>2</sub>O<sub>3</sub> powder (FeS<sub>x</sub>/Al<sub>2</sub>O<sub>3</sub>) with our ALD process at 160 °C (1500 cycles) under the same deposition conditions. Additional characterization (Figure S4) confirmed that the FeS<sub>x</sub> films deposited on Al<sub>2</sub>O<sub>3</sub> substrates had very similar material properties to those deposited on SiO<sub>2</sub>. The deposition produced a mass load of 1.1 wt % of FeS<sub>x</sub>, as determined by dissolving the product powder in acid solution and measuring the iron amount by atomic emission spectroscopy. SEM in combination with energy-dispersive X-ray spectroscopy (EDS) was used to examine the elemental composition of the ALD-prepared FeS<sub>x</sub>/Al<sub>2</sub>O<sub>3</sub> powder. As shown in Figure 6, benefited from the self-limiting growth behavior, in the ALD-prepared FeS<sub>x</sub>/Al<sub>2</sub>O<sub>3</sub> powder, Fe and S were highly uniformly distributed on the Al<sub>2</sub>O<sub>3</sub> powder, which highlighted the advantageous properties of ALD for synthesizing uniform catalysts (see also Figures S5 and S6).

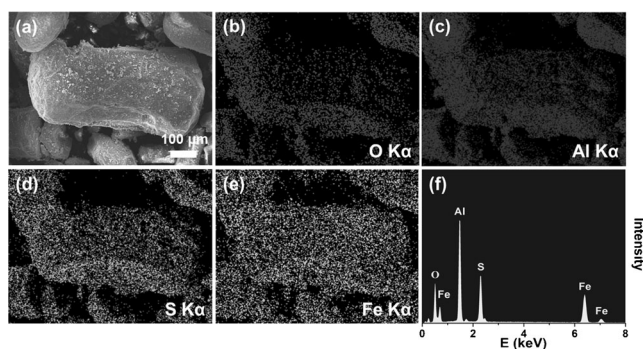


**Figure 6.** a) Representative SEM image of an ALD-prepared FeS<sub>x</sub>/Al<sub>2</sub>O<sub>3</sub> powder. b) O, c) Al, d) S, and e) Fe EDS elemental distributions of the FeS<sub>x</sub>/Al<sub>2</sub>O<sub>3</sub> powder imaged in (a). f) The corresponding EDS spectrum.

The ALD FeS<sub>x</sub>/Al<sub>2</sub>O<sub>3</sub> material was used as a catalyst in the selective reduction (hydrogenation) of various azobenzenes into the corresponding hydrazobenzenes with sodium borohydride (NaBH<sub>4</sub>) as the hydrogen source. As the simplest compound of this class, azobenzene was effectively reduced to hydrazobenzene at room temperature with 97% conversion and >99% selectivity within 20 min with only 0.9 mol % of the ALD FeS<sub>x</sub>/Al<sub>2</sub>O<sub>3</sub> catalyst (Table 1, entry 1). To compare the catalyst performance, various control experiments were performed in parallel and under the same reaction conditions. As shown in Table 1, the reactions without any catalyst (entry 2) or with uncoated  $\gamma$ -Al<sub>2</sub>O<sub>3</sub> powder (entry 3) barely produced any product (<5% conversion). Commercial Fe<sub>2</sub>O<sub>3</sub> powder (entry 4) and FeCl<sub>2</sub> (entry 5) catalyzed the reaction to some extent, but both of them were much less effective, with only 17 and 25% conversion, respectively, than our ALD FeS<sub>x</sub>/Al<sub>2</sub>O<sub>3</sub> catalyst. Solvothermally synthesized<sup>[22]</sup> mackinawite FeS<sub>x</sub> nanoparticles (s-FeS<sub>x</sub>(m), entry 6) were also used

**Table 1:** Comparison of the catalytic performance of ALD FeS<sub>x</sub>/Al<sub>2</sub>O<sub>3</sub> and other catalysts in the hydrogenation of azobenzene (2.0 mmol) at room temperature.

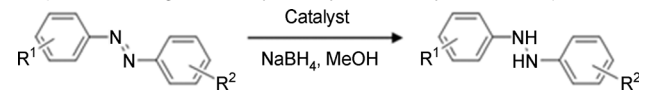
Entry	Catalyst (mol %) <sup>[a]</sup>	Conv. [%]	Selectivity [%]	Molar TOF <sup>[b]</sup> [h <sup>-1</sup> ]	Areal TOF <sup>[b]</sup> [mmol h <sup>-1</sup> m <sup>-2</sup> ]
1	ALD FeS <sub>x</sub> /Al <sub>2</sub> O <sub>3</sub> (0.9)	97	>99	323	533
2	–	<5	–	–	–
3	Al <sub>2</sub> O <sub>3</sub>	<5	–	–	–
4	Fe <sub>2</sub> O <sub>3</sub> (10)	17	98	5.0	5.5
5	FeCl <sub>2</sub> (10)	25	>99	7.5	– <sup>[c]</sup>
6	s-FeS <sub>x</sub> (m) (10)	61	97	17.8	46.7
7	s-FeS <sub>x</sub> (m)+Al <sub>2</sub> O <sub>3</sub> (10)	63	96	18.1	47.5
8	s-FeS <sub>x</sub> (p) (10)	55	>99	16.3	89.6

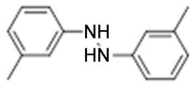
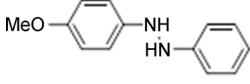
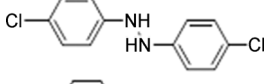
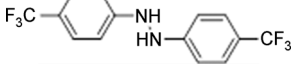
[a] The amount of catalyst with respect to azobenzene. [b] The molar (areal) TOF corresponds to the number of moles of converted hydrazobenzene per unit time per mole (unit area) of catalyst. The calculations are detailed in the Supporting Information. [c] Soluble in MeOH.

for comparison, but at a fairly high catalyst loading (10 mol %); however, the reaction conversion was much lower (67%), and an appreciable amount (3%) of over-reduced byproduct (aniline) was also formed at the same time. A mixture of solvothermally synthesized FeS<sub>x</sub>(m) and  $\gamma$ -Al<sub>2</sub>O<sub>3</sub> powder (entry 7) basically gave the same catalytic performance as the s-FeS<sub>x</sub>(m) alone, which ruled out any synergistic effects between the FeS<sub>x</sub> layer and  $\gamma$ -Al<sub>2</sub>O<sub>3</sub> powder. Pyrrhotite FeS<sub>x</sub> nanowires (s-FeS<sub>x</sub>(p)) were also solvothermally synthesized<sup>[23]</sup> for comparison (entry 8), but the reaction conversion was even lower (55%) despite the high catalyst loading (10 mol %). Additional comparisons with various other reported catalysts are provided in Table S1. The reaction turnover frequencies (TOFs) were also calculated with respect to both the molar amount and the surface area of each catalyst. The ALD FeS<sub>x</sub>/Al<sub>2</sub>O<sub>3</sub> catalyst gave rise to the best molar and areal TOFs among the catalysts shown in Table 1. Therefore, we have clearly demonstrated the superior catalytic performance of ALD FeS<sub>x</sub>/Al<sub>2</sub>O<sub>3</sub> in the hydrogenation of azobenzene.

We further extended the evaluation of the ALD FeS<sub>x</sub>/Al<sub>2</sub>O<sub>3</sub> catalyst to a broader range of azobenzene derivatives. As listed in Table 2, at a low catalyst loading (ca. 1 mol %), a variety of azobenzenes with methyl, methoxy, chloro, or trifluoromethyl substituents were selectively (>99%) reduced to the corresponding hydrazobenzenes with fairly good conversions. These results clearly demonstrate the broad applicability of this ALD FeS<sub>x</sub>/Al<sub>2</sub>O<sub>3</sub> catalyst as both electron-donating and electron-withdrawing substituents were well tolerated. In addition, the ALD FeS<sub>x</sub>/Al<sub>2</sub>O<sub>3</sub> catalyst could also be recycled and reused for quite a few runs. Taking azobenzene as an example, the recollected catalyst still showed excellent product selectivity (>99%) and fairly high conversions of 91 and 88% in the second and third reaction run, respectively. Although further mechanistic studies are needed, the superior catalytic performance of ALD FeS<sub>x</sub>/Al<sub>2</sub>O<sub>3</sub> is perhaps related to the special properties of the ALD FeS<sub>x</sub> material. Benefitting from the merits of ALD for highly conformal coatings with superb reproducibility

**Table 2:** Hydrogenation of substituted azobenzenes (2.0 mmol) at room temperature using ALD FeS<sub>x</sub>/Al<sub>2</sub>O<sub>3</sub> (ca. 1 mol%) as the catalyst.<sup>[a]</sup>



Entry	Product	t [min]	Conv. [%]
1		20	93
2		30	67
3		20	80
4		10	98

[a] For all reactions in this Table, the selectivity was > 99%.

bility, this catalyst material could be uniformly loaded onto the support substrate, which highlights the important role of ALD for the reproducible fabrication of uniform supported catalysts for organic synthesis.

In summary, we have reported a new ALD process for the synthesis of FeS<sub>x</sub> from bis(*N,N'*-di-*tert*-butylacetamidinato)iron(II) and H<sub>2</sub>S. The ALD process follows ideal self-limiting ALD growth behavior to produce fairly pure, smooth, and well-crystallized FeS<sub>x</sub> films. The ALD FeS<sub>x</sub> films could also be conformally deposited into deep narrow trenches with aspect ratios as high as 10:1, which indicates that this ALD process is highly suitable for preparing conformal and uniform FeS<sub>x</sub> coatings on porous or complex 3D nanostructures in general. Therefore, this process will have a broad scope of applications in nanoscience and nanoengineering. We further demonstrated its promising application by the preparation of uniform nanoscale FeS<sub>x</sub> coatings on porous  $\gamma$ -Al<sub>2</sub>O<sub>3</sub> powder. The ALD FeS<sub>x</sub>/Al<sub>2</sub>O<sub>3</sub> catalyst exhibited excellent catalytic activity and selectivity in the hydrogenation of azobenzenes to hydrazobenzene derivatives under mild reaction conditions, which demonstrates the high promise of ALD FeS<sub>x</sub> in organic synthesis.

## Acknowledgements

This work was financially supported by the NSFC (51672011, 21601006), the Guangdong Natural Science Funds for Distinguished Young Scholars (2015A030306036), Guangdong Innovation Team Project (2013N080), and the Shenzhen Science and Technology Innovation Committee (KQCX20150327093155293).

## Conflict of interest

The authors declare no conflict of interest.

**Keywords:** atomic layer deposition · hydrogenation · iron · supported catalysts · thin films

- [1] a) J. Puthussery, S. Seefeld, N. Berry, M. Gibbs, M. Law, *J. Am. Chem. Soc.* **2011**, *133*, 716–719; b) Y.-C. Wang, D.-Y. Wang, Y.-T. Jiang, H.-A. Chen, C.-C. Chen, K.-C. Ho, H.-L. Chou, C.-W. Chen, *Angew. Chem. Int. Ed.* **2013**, *52*, 6694–6698; *Angew. Chem.* **2013**, *125*, 6826–6830; c) N. Berry, M. Cheng, C. L. Perkins, M. Limpinsel, J. C. Hemminger, M. Law, *Adv. Energy Mater.* **2012**, *2*, 1124–1135.
- [2] a) C. Xu, Y. Zeng, X. Rui, N. Xiao, J. Zhu, W. Zhang, J. Chen, W. Liu, H. Tan, H. H. Hng, Q. Yan, *ACS Nano* **2012**, *6*, 4713–4721; b) S.-B. Son, T. A. Yersak, D. M. Piper, S. C. Kim, C. S. Kang, J. S. Cho, S.-S. Suh, Y.-U. Kim, K. H. Oh, S.-H. Lee, *Adv. Energy Mater.* **2014**, *4*, 1300961; c) C. Zhu, Y. Wen, P. A. van Aken, J. Maier, Y. Yu, *Adv. Funct. Mater.* **2015**, *25*, 2335–2342.
- [3] a) D. Kong, J. J. Cha, H. Wang, H. R. Lee, Y. Cui, *Energy Environ. Sci.* **2013**, *6*, 3553–3558; b) M. S. Faber, M. A. Lukowski, Q. Ding, N. S. Kaiser, S. Jin, *J. Phys. Chem. C* **2014**, *118*, 21347–21356; c) D.-Y. Wang, M. Gong, H.-L. Chou, C.-J. Pan, H.-A. Chen, Y. Wu, M.-C. Lin, M. Guan, J. Yang, C.-W. Chen, Y.-L. Wang, B.-J. Hwang, C.-C. Chen, H. Dai, *J. Am. Chem. Soc.* **2015**, *137*, 1587–1592; d) D. Jasion, J. M. Barforoush, Q. Qiao, Y. Zhu, S. Ren, K. C. Leonard, *ACS Catal.* **2015**, *5*, 6653–6657.
- [4] M. Shen, C. Ruan, Y. Chen, C. Jiang, K. Ai, L. Lu, *ACS Appl. Mater. Interfaces* **2015**, *7*, 1207–1218.
- [5] A. Roldan, N. Hollingsworth, A. Roffey, H. U. Islam, J. B. M. Goodall, C. R. A. Catlow, J. A. Darr, W. Bras, G. Sankar, K. B. Holt, G. Hogarth, N. H. de Leeuw, *Chem. Commun.* **2015**, *51*, 7501–7504.
- [6] a) H. Seino, M. Hidai, *Chem. Sci.* **2011**, *2*, 847–857; b) T. B. Nguyen, L. Ermolenko, A. Al-Mourabit, *J. Am. Chem. Soc.* **2013**, *135*, 118–121.
- [7] a) M. R. Gao, Y. F. Xu, J. Jiang, S. H. Yu, *Chem. Soc. Rev.* **2013**, *42*, 2986–3017; b) X. Rui, H. Tan, Q. Yan, *Nanoscale* **2014**, *6*, 9889–9924.
- [8] a) M. Cabán-Acevedo, M. S. Faber, Y. Tan, R. J. Hamers, S. Jin, *Nano Lett.* **2012**, *12*, 1977–1982; b) M. Cabán-Acevedo, D. Liang, K. S. Chew, J. P. DeGrave, N. S. Kaiser, S. Jin, *ACS Nano* **2013**, *7*, 1731–1739; c) D. R. Cummins, H. B. Russell, J. B. Jasinski, M. Menon, M. K. Sunkara, *Nano Lett.* **2013**, *13*, 2423–2430.
- [9] a) L. Samad, M. Cabán-Acevedo, M. J. Shearer, K. Park, R. J. Hamers, S. Jin, *Chem. Mater.* **2015**, *27*, 3108–3114; b) K. Ramasamy, M. A. Malik, M. Helliwell, F. Tuna, P. O'Brien, *Inorg. Chem.* **2010**, *49*, 8495–8503.
- [10] C. Marichy, M. Bechelany, N. Pinna, *Adv. Mater.* **2012**, *24*, 1017–1032.
- [11] a) S. M. George, *Chem. Rev.* **2010**, *110*, 111–131; b) R. W. Johnson, A. Hultqvist, S. F. Bent, *Mater. Today* **2014**, *17*, 236–246.
- [12] a) B. Ahmed, C. Xia, H. N. Alshareef, *Nano Today* **2016**, *11*, 250–271; b) X. Meng, X.-Q. Yang, X. Sun, *Adv. Mater.* **2012**, *24*, 3589–3615.
- [13] B. J. O'Neill, D. H. K. Jackson, J. Lee, C. Canlas, P. C. Stair, C. L. Marshall, J. W. Elam, T. F. Kuech, J. A. Dumesic, G. W. Huber, *ACS Catal.* **2015**, *5*, 1804–1825.
- [14] a) J. Lu, B. Fu, M. C. Kung, G. Xiao, J. W. Elam, H. H. Kung, P. C. Stair, *Science* **2012**, *335*, 1205–1208; b) C. P. Canlas, J. Lu,

- N. A. Ray, N. A. Grosso-Giordano, S. Lee, J. W. Elam, R. E. Winans, R. P. Van Duyne, P. C. Stair, J. M. Notestein, *Nat. Chem.* **2012**, *4*, 1030–1036; c) J. E. Mondloch, W. Bury, D. Fairen-Jimenez, S. Kwon, E. J. DeMarco, M. H. Weston, A. A. Sarjeant, S. T. Nguyen, P. C. Stair, R. Q. Snurr, O. K. Farha, J. T. Hupp, *J. Am. Chem. Soc.* **2013**, *135*, 10294–10297; d) S. Hu, M. R. Shaner, J. A. Beardslee, M. Lichterman, B. S. Brunshwig, N. S. Lewis, *Science* **2014**, *344*, 1005–1009; e) S. Mubeen, J. Lee, N. Singh, S. Kramer, G. D. Stucky, M. Moskovits, *Nat. Nanotechnol.* **2013**, *8*, 247–251.
- [15] V. Miikkulainen, M. Leskela, M. Ritala, R. L. Puurunen, *J. Appl. Phys.* **2013**, *113*, 021301.
- [16] N. P. Dasgupta, X. Meng, J. W. Elam, A. B. F. Martinson, *Acc. Chem. Res.* **2015**, *48*, 341–348.
- [17] T. L. Gilchrist in *Comprehensive Organic Synthesis* (Ed.: I. Fleming), Pergamon, Oxford, **1991**, pp. 381–402.
- [18] L. G. Benning, R. T. Wilkin, H. L. Barnes, *Chem. Geol.* **2000**, *167*, 25–51.
- [19] M. Wolthers, L. Charlet, P. R. van Der Linde, D. Rickard, C. H. van Der Weijden, *Geochim. Cosmochim. Acta* **2005**, *69*, 3469–3481.
- [20] A. F. Guillermet, M. Hillert, B. Jansson, B. Sundman, *Metall. Trans. B* **1981**, *12*, 745–754.
- [21] H. Li, Y. Gao, Y. Shao, Y. Su, X. Wang, *Nano Lett.* **2015**, *15*, 6689–6695.
- [22] I. T. Sines, D. D. Vaughn Ii, R. Misra, E. J. Popczun, R. E. Schaak, *J. Solid State Chem.* **2012**, *196*, 17–20.
- [23] M. Nath, A. Choudhury, A. Kundu, C. N. R. Rao, *Adv. Mater.* **2003**, *15*, 2098–2101.

Manuscript received: January 14, 2017

Final Article published: ■ ■ ■ ■, ■ ■ ■ ■ ■

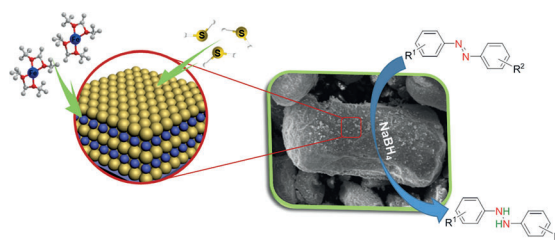
## Communications



## Atomic Layer Deposition

Y. Shao, Z. Guo, H. Li, Y. Su,  
X. Wang\* ————— ■■■■-■■■■

Atomic Layer Deposition of Iron Sulfide  
and Its Application as a Catalyst in the  
Hydrogenation of Azobenzenes



Iron sulfide ( $\text{FeS}_x$ ) thin films were  
obtained by atomic layer deposition.  
Nanoscale  $\text{FeS}_x$  coatings on porous  $\gamma$ -

$\text{Al}_2\text{O}_3$  powder were also prepared and  
showed excellent catalytic activity and  
selectivity in azobenzene hydrogenation.